SYNTHESIS REPORT FOR PUBLICATION

CONTRACT N⁰	**BREU-CT90-0338**
PROJECT N⁰	**BE-0338**
TITLE	INITIATION AND GROWTH OF **THERMO-**MECHANICAL FATIGUE CRACKS IN COATED AND UNCOATED TURBINE BLADE MATERIALS
PROJECT COORDINATOR	**Rolls-Royce plc, UK**
PARTNERS	**MTU Motoren-und Turbinen-Union München, Germany** **Centro de Estudios e Investigaciones Tecnicas de Guipuzcoa (CEIT), Spain**
SUBCONTRACTOR	**Joint Research Centre, EC-Petten, The Netherlands**
STARTING DATE	**1 January 1991**
DURATION	***54*** **months**

PROJECT FUNDED BY THE EUROPEAN COMMUNITY UNDER THE BRITE/EURAM PROGRAMME

Date: January 8,1996

INITIATION AND GROWTH OF THERMO-MECHANICAL FATIGUE CRACKS IN COATED AND UNCOATED TURBINE BLADE MATERIALS

J.Bressers[1], A.Bennett[2], E. E. Affeldt[3], J.M.Martinez-Esnaola[4]

[1] JAM, JRC, P. O. Box 2, 1755 ZG, Petten, The Netherlands
[2] Rolls-Royce plc, P. O.Box 31, Derby DE24 8BJ, United Kingdom
[3] MTU Motoren und Turbinen Union,Postfach 500640,80976 München, Germany
[4] CEIT, Paseo de Manuel Lardizabal 15, E-20009 San Sebastian, Spain

ABSTR4CT

In aero gas turbine blades coatings are used in order to provide the blades with adequate protection against environmental degradation. Issues of major concern in blade design are the effect of therms.l+fatigue on the operational life of coated blades, and the availability of an adequate life prediction model.

This paper reports the results of a study evaluating the effect of various diffusion and overlay coatings on microcrack initiation, on crack growth and on the total life of the single crystal nickel-based superalloys SRR99 and CMSX6 under thermo-mechanical fatigue (TMF) loading. Different TMF cycle types with a minimum temperature of 300°C and maximum temperatures of 850°C and 105O"C, and with different minimum-to-maximum strain ratios were used to simulate the thermal and mechanical loads on volume elements identified as critical by means of Finite Element analysis of blades. With some exceptions, coatings are found to have a detrimental effect on the TMF life, although under specific conditions aluminide coatings in particular turn out to delay the initiation of microcracks as compared" to the uncoated single crystal material. Evaluation of the crack initiation and growth mechanisms provides a basis for the definition of some measures for improving the performance of the coated materials. Lines are suggested along which further work must proceed in order to gain a fuller understanding of coated blade behaviour, thereby enabling the tailoring of coating composition and microstructure for optimum performance.

Since the major part of the TMF life is spent in crack growth, life prediction is based on mechanism-informed crack growth modelling. As a precursor to TMF crack growth modelling, a fatigue-oxidation model describing crack growth under isothermal loading conditions over a wide range of temperatures and loading rates is developed. Because different darnage mechanisms operate during loading with different TMF cycle types, the formulation of a generally applicable life prediction model for TMF is precluded. The crack growth model proposed in this paper applies to -135° out-of-phase TMF cycling, which turned out to be the most critical cycle in terms of TMF Life. The model accounts for the differences in life between uncoated and nickel-aluminide coated SRR99 through the smaller crack closure effects in the coated specimens which result from a smaller oxidation influence as compared to uncoated material.

1. INTRODUCTION

High and intermediate pressure blades of aero gas turbines are made of single crystal nickel based alloys, microstructurally designed to retain strength up to high temperatures. Various protective measures are taken to guarantee efficient operation of the blades up to service temperatures which may be as high as 1130°C. The provision of internal cooling holes limits the blade's maximum service temperature, whereas surface coatings inhibit the blade material from being degraded by the oxidising burner gas environment. The major cause of failure in current single crystal blades of aero gas turbines are thermally induced stresses, which result from thermal strains over the blade thickness caused by temperature gradients during heating and cooling cycles, in particular during the acceleration and deceleration stages of the flight cycle. The blade design, in combination with the transient temperature and mechanical loading conditions, and the presence of coatings set a complex mix of material degradation mechanisms

into operation which eventually lead to the loss of integrity of the blade/coating composite. These mechanisms must be identified, assessed and evaluated in order to build a reliable life prediction model, to optimise the operation conditions of the blades for minimum damage, and to enable tailoring of, the microstructure/chemical composition of the substrate and of the coating towards better, performance. Isothermal mechanical fatigue data, which are traditionally used for blade design purposes, do not account for the darnage and failure processes occurring in blades exposed to thermal fatigue cycles. Moreover, blades provided with relatively brittle coatings are expected to display a non-isothermal fatigue behaviour because of the ductile-brittle transition of the coating at intermediate temperatures. Actual blade behaviour is more closely simulated by thermo-mechanical fatigue (TMF) tests, which are designed to reproduce the temperature and strain cycles seen by critical volume elements of the blade.

The current project had the following objectives. First, to create from a matrix of TMF experiments, a data base of behavioral relationships from which a qualitative understanding of the primary mechanisms involved in blade degradation and failure would evolve. Second, to use this knowledge to construct a quantitative predictive model which would encapsulate the understanding.

2. TECHNICAL DESCRIPTION

2.1. MATERIALS

Two single crystal materials of industrial quality are used as substrate materials, i.e. SRR99 and CMSX6. The corresponding chemical compositions are presented in Table 1. The crystallographic orientation of the long axis (stress axis) of the test specimens is within 12° of <001>. SRR99 was coated with a high activity nickel-aluminide diffusion coating (NiAl), and with vacuum plasma sprayed CoNiCrAlY and Re/Si modified CoNiCrAlY overlay coatings. The coating applied to CMSX6 was a modified diffusion type coating, PtAl. Both the coated and uncoated test specimens were given the standard coating and ageing heat treatments. The surface finish in the gauge length of the substrate material is R_a=0.05 µm. Coated specimens are tested in the as received condition without any further surface modification treatment.

TABLE l-Chemical composition of SRR99 and CMSX6 (in wt.%)

	Al	Co	Cr	Mo	Ta	Ti	W	c	Ni
SRR99	5.3	4.8	8.25	0.5	2.65	2.05	9.25	.015	bal.
CMSXY6	4.85	5.0	10.0	3,0	2.0	4.75	-	.006	bal.

2.2. ANALYSIS OF BLADE CYCLES

3-D Finite Element analysis of blade elements at the leading edge, trailing edge and pressure surface-mid chord was performed on high pressure first stage and on second stage turbine blades, without making an allowance for the presence of the coating. From these numerical results, two idealised TMF cycle types were devised for use in the TMF tests, see fig. 1, representing in-phase and out-of-phase strain-temperature conditions. For the out-of-phase cycle (- 135 °lag) two variants with different values of the strain ratios R are used i.e. R=-∞ (simulating a hot spot condition) and R=O. The strain ratio R equals zero in the case of the in-phase tests. The minimum cycle temperature is 300°C. The maximum cycle temperature varies from 850°C in the in-phase tests to 105O”C in the - 135°lag tests. A series of tests with 300 s holdtimes at the maximum cycle temperature were included in the TMF testing matrix. The type of damage observed on blades following engine demonstrator tests is also observed on the TMF tested specimens, pointing out that the idealised TMF cycle correctly mimics the in-service damage mechanisms.

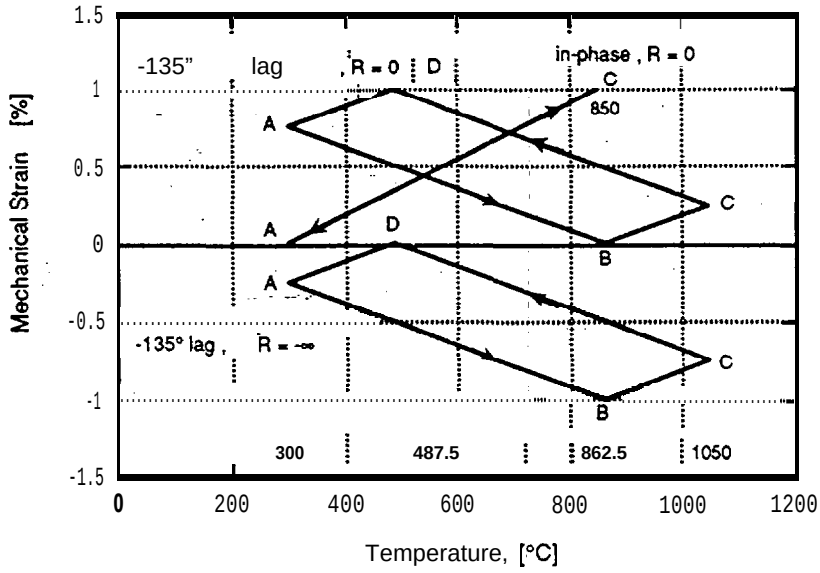

Fig. 1. TMF cycle types

2.3. THERMO-MECHANICAL FATIGUE

The TMF tests are carried out in total strain control between mechanical strain limits on computer controlled universal testing machines. The test specimen is heated by means of direct electromagnetic induction. The temperature is varied linearly with time and synchronously in-phase, or with a 135° phase lag with respect to the mechanical strain. The mechanical strain ε_m is defined as

$$\varepsilon = \varepsilon_m - \varepsilon_{th} = \sigma/E + \varepsilon_{in} - \varepsilon_{th} \quad (1)$$

where $\varepsilon, \varepsilon_{th}$ and&h are the total, thermal and inelastic components of the strain, and σ/E is the elastic strain component (σ is stress, E is Young's modulus). Prior to each TMF test the temperature dependence of the E-modulus for the test specimen involved is measured at intervals of 100"C, up to the maximum temperature of the TMF cycle. The thermal expansion of the specimen is recorded as a continuous function of the temperature whilst heating and cooling the specimen at the same rate as in the actual TMF test.

In order to approach in-service heating and cooling rates of blades as realistically as possible, specimen heating and cooling rates were equal to or in excess of 10°C/s. Forced cooling during the larger part of the downward branch of the cycle is required in order to enable the cooling rate to be achieved. The mechanical strain rates range between approximately 3x10-5 s^{-1} and 1.5x 10^{-5} s-l. All the regular TMF tests are started at 300°C whilst in some of the - 135°1ag, R=O tests the TMF sequence was started at 862°C where ε_m=0 (hot start).

Crack initiation and the growth history of individual microcracks are monitored by means of a computer vision system, allowing the contactless, in-situ and fully automated measurement of the microcracking process, at a magnification which enables microcracks of approximately l=15-30 μm length at the surface to be detected under the oxidizing conditions of the test. The images are digitized and stored for post processing.

2.4. ISOTHERMAL CRACK GROWTH

In addition to TMF tests, isothermal crack growth tests were performed to investigate the influence of time, temperature and R-ratio on the crack growth rate. Use was made of corner-

cracked (CC) test specimens of rectangular cross-section, with starter cracks of 50-100 μm deep. Crack propagation in the <100> direction was measured by means of a DC potential drop technique. The standard loading cycle was trapezoidal with uploading, dwell at maximum load, downloading and dwell at minimum load of one second each (1/1/1/1 type cycle). A triangular loading cycle with up- and downloading times equal to the standard TMF cycle was used to investigate" the time dependence of the crack growth rate. The stress ratio R was maintained at R=O or R=-0.5. The stress intensity factors are calculated according to [1].

3. RESULTS

In this section a summary of the major project results is presented. The experimental results are illustrated by means of a few-selected examples. For more detailed information regarding specific aspects of the experimental results concerning TMF and their interpretation, the reader is referred to references [2] to [5]. References [6] to [16], which are the result of related work performed within the framework of the JRC specific programme, provide information concerning issues related to the evolution of the microstructure of single crystal materials and coatings. Ref. [17] relates to the crack growth in uncoated SRR99 and CMSX6 under isothermal conditions. "The major results in terms of lifetime prediction concern the modelling of isothermal crack growth and the prediction of crack growth under TMF conditions. The corresponding project results are published in more detail in references [18] to [24].

3.1. EXPERIMENTAL RESULTS

3.1.1 Stress-strain behaviour during TMF

Strain controlled TMF cycling of the single crystal nickel-based alloys provokes a pronounced shift of the cyclic stresses early in the cyclic life, followed either by a saturation stage or by a more gradual change in stress from approximately $N/N_f \approx 0.1$ onwards. N_f is the total life defined as the cycle number at which the stress has dropped to 2/3 of the saturation level. The observed hardening is kinematic. The direction and the degree of the primary and secondary stages of the cyclic hardening/softening depend on the type of TMF cycle, on the applied strain range and on whether the cycle contains a hold time. The cyclic hardening results from the accumulation of inelastic deformation on a cycle-by-cycle basis, caused by plasticity and/or creep. Detailed evaluation of each cycle shows that inelastic deformation of the material is limited to specific ternperature/stress regimes within the cycle. For example, fig.2 (right) documents the stresses and temperatures as a function of time in the first cycle of the -135°lag,R=-∞ TMF test for a strain level of $\Delta\varepsilon_m$=1%. The TMF cycle stresses are compared to the stress required for achieving 0.1 % plastic strain (O. 1 % PS) at the corresponding temperature. In addition the average primary creep rate corresponding to the momentary TMF cycle stress and temperature is plotted. Inelastic deformation occurs when the cycle stress equals the 0.1 % PS level and/or when it reaches a level where the creep contribution becomes significant. Large scale plastic deformation in compression starts at a temperature of nearly 850°C and ends just beyond T_{max}. The high average creep rate shown in fig.2 results from the combination of high stress and temperature during this part of the cycle. The pronounced primary hardening is the result of re-establishing the prescribed mechanical strain levels during subsequent cycles. However, with increasing cycle number the compressive cycle stresses which drive the inelastic deformation rapidly drop to small absolute values, eventually ceasing to cause further build-up of inelastic strain from $N/N_f \approx 0.1$ onwards, see fig.2 (left). In contrast to the R=-∞ condition, in the - 135°1ag, R=O cycle test the accumulation of tensile inelastic strain is primarily due to plastic deformation in tension in the temperature range 650°C to 350°C. In the in-phase tests plastic deformation in the high temperature part of the TMF cycle drives the pronounced primary tensile softening/compressive hardening, whilst a gradual yet steady accumulation of the inelastic strain between $N/N_f \approx 0.1$ and $N/N_f \approx 0.9$ continues after this stage, primarily as the result of creep deformation. The pronounced inelastic deformation early in life in each type of TMF test generally results in a shakedown of the cyclic stresses to values close to the elastic regime, yielding nearly closed stress-strain loops during the major fraction of life. The different mechanisms of damage accumulation operating in the different TMF cycle types preclude the formulation of a generally applicable life prediction model for these first stages of Me.

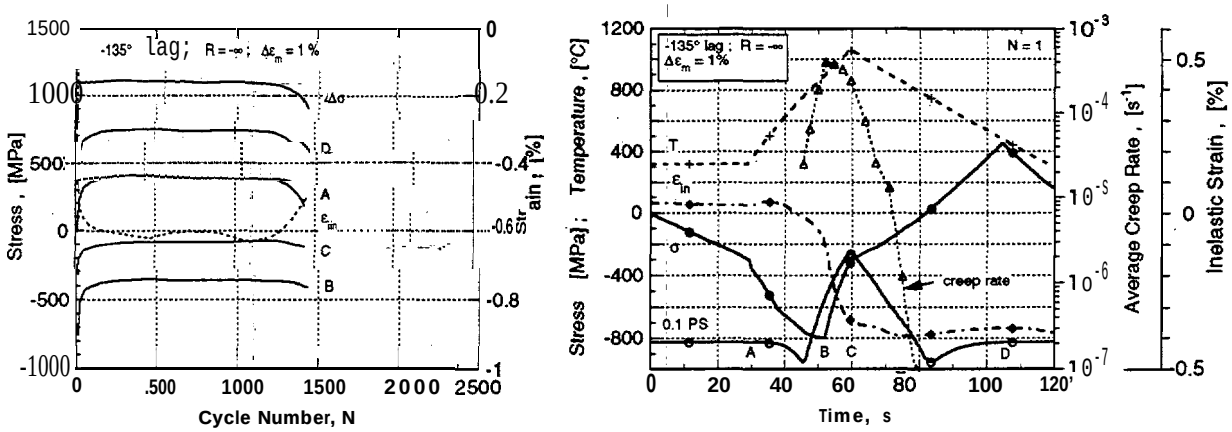

Fig.2. Stress, temperature and inelastic strain as a 'function of time in the first cycle of the -135°lag,R=-∞ TMF test at a strain level of $\Delta\varepsilon_m$=1 %. The stress for 0.190 plastic deformation (O. lPS) and the average primary creep rate are included for comparison (right). Evolution of the characteristic cycle stresses (see fig. 1 for the meaning of A to D) and of the corresponding inelastic strain with cycle number N (left).

3.1.2. TMF crack initiation versus total life

The number of cycles at which the surface length l of the crack has reached 30pm (corresponding to a crack depth a_i=15μm) is defined as initiation N_i, although frequently cracks are first detected at smaller cycle numbers. For the in-phase tests precise N_i data are not available because of their sub-surface initiation. A conservative estimate of N_i/N_f, based on the observation of the first surface breaking of sub-surface initiated cracks, suggests $N_i/N_f<0.3$.

Analysis of the computer vision images shows that cracks initiate very early in the cyclic life. As an example crack initiation data, N_i, and total life data, N_f, are presented in graphical form in Fig.3 as a function of the applied mechanical strain range $\Delta\varepsilon_m$.

In the - 135°lag tests microcrack initiation starts at life fractions in the range $0.01 \le N_i/N_f \le 0.1$. For the - 135°lag,R=-∞ TMF cycle, coating of SRR99 with CoNiCrAlY retards crack initiation at low levels of Δe_m as compared "to uncoated SRR99, whilst sharply reducing the number of cycles required to grow the major crack to failure of the specimen. As a result, the total life N_f is reduced by a factor of 5. At high $\Delta\varepsilon_m$ the overlay coated specimens display equal N_i and a slightly longer total life as compared to uncoated material, The lives of the Re/Si modified and of the standard CoNiCrAlY coated specimens are comparable. The NiAl coating on SRR99 results in a reduction of N_i at strain ranges $\Delta\varepsilon_m \ge 0.8\%$, but has an increasingly beneficial effect at smaller $\Delta\varepsilon_m$ levels. In terms of total life a small yet consistent reduction relative to uncoated SRR99 is observed at all $\Delta\varepsilon_m$ levels. The presence of PtAl on CMSX6 has the effect of causing a ten-fold increase of N_i relative to uncoated CMSX6 when $\Delta\varepsilon_m \le 0.8\%$, resulting in longer total lives of the coated specimens at strain ranges $\le 0.7\%$. The -135° lag, R=O cycle is more damaging than the R=-∞ cycle in terms of crack initiation for both NiAl and MCrAlY coated SRR99, whilst the reverse holds for uncoated SRR99.

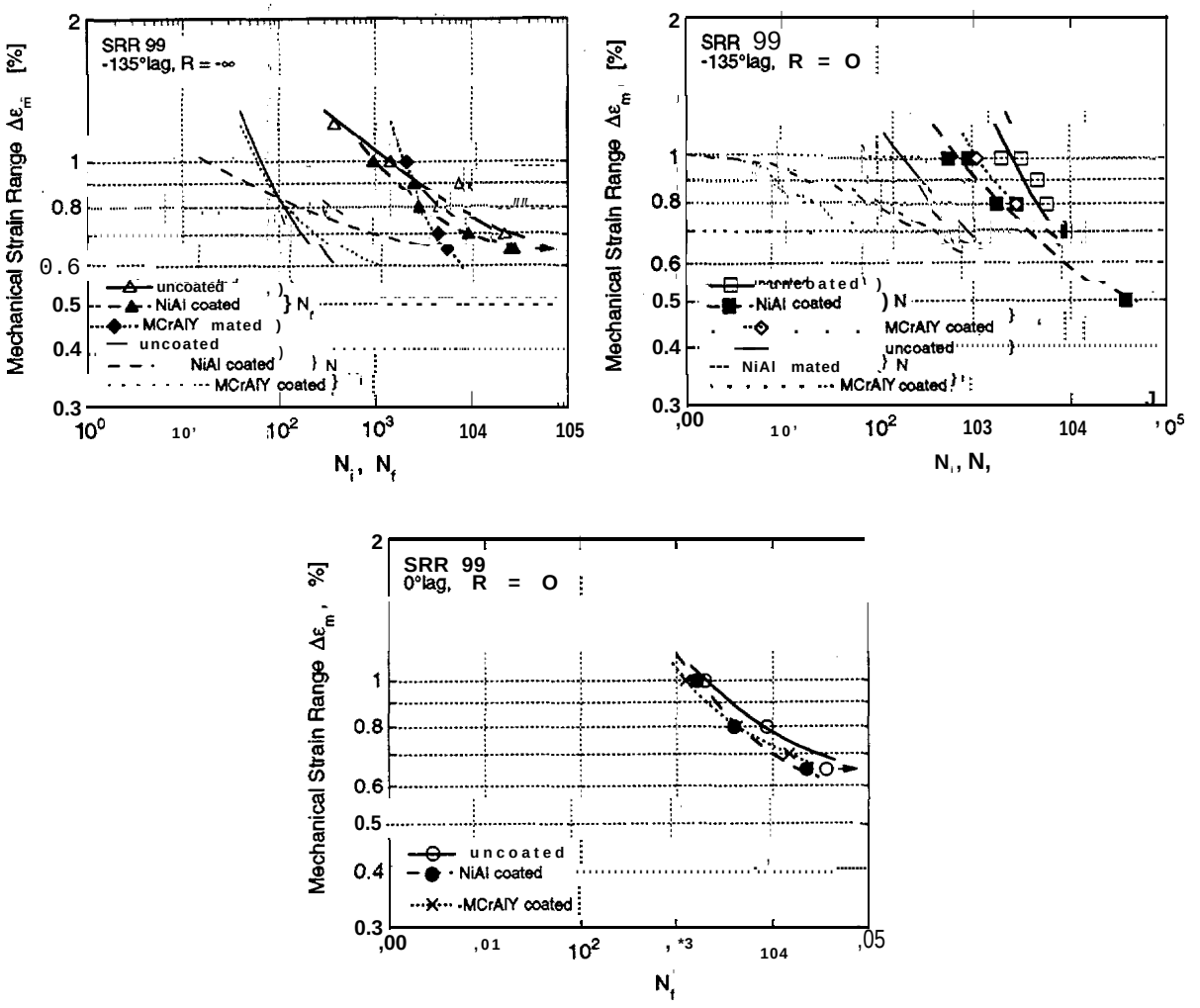

Fig. 3. Crack initiation lives N_i and total lives N_f versus $\Delta\varepsilon_m$

In terms of total life, R=-∞ cycling yields longer lives than R=O cycling in NiAl coated SRR99 irrespective of the applied strain range, whereas a cross-over from longer to shorter lives is observed with decreasing strain range in uncoated and MCrAlY coated SRR99. For the in-phase tests, N_f of the coated SRR99 is about half the life of bare SRR99 at small strain ranges, whilst at AE.=170 approximately equal lives are measured. PtAl coated and uncoated CMSX6 display nearly equal lives for in-phase loading. Adding a 300s holdtime at the maximum cycle temperature leads to a substantial life reduction in the uncoated materials at the high strain ranges as the result of oxidation accelerated crack growth. The life reduction factor becomes smaller with decreasing $\Delta\varepsilon_m$. However, in PtAl coated CMSX6 the addition of a holdtime to the TMF cycle results in an increasing life reduction with decreasing strain range.

Cracks continue to initiate during the later stages of the -135°lag TMF tests, albeit that the crack number densities evolve differently with cycling for coated and uncoated materials. For example, in uncoated SRR99 the crack number density n rises sharply up to a life fraction $N/N_f \approx 0.1$, and subsequently saturates at about 30 cracks/cm^2. The steep rise of n corresponds with the stage of pronounced cyclic hardening early in life during which the cyclic stress levels increase sharply with increasing N whilst the stress range $\Delta\sigma$ remains constant.;-

Crack initiation in the uncoated materials appears frequently to be associated with the preferential oxidation of microstructural features located in stringers along the long axis of the test specimen, resulting in oxide hillocks protruding from the surface which are cracked. There is evidence that these preferred sites of crack initiation which are located in the interdendritic zones, are associated, with casting porosity and/or carbides. At strain ranges in excess of approximately 170, large scale slip on a preferred slip: plane may trigger cracks to initiate and

grow in the crystallographic stage I. In NiAl coated SRR99 and in PtAl coated CMSX6 brittle failure of the coating is observed under -135°lag cycling at strain ranges in excess of about 0.8%, changing to a ductile mode of crack initiation yielding multiple penny shaped cracks at lower strain ranges. The transition strain level is in line with the coating failure strain of 0.8% at temperatures below the DBTT of the coating, as measured in tension tests on NiAl coated SRR99. The longer lives measured in hot start versus cold start tests corroborate the idea that the residual strains in the coating relax at the high temperature end of the TMF cycle. Microstructural analysis of the cracking locations in NiAl coated SRR99 suggests that the cracking process is exacerbated by the presence of the strain concentrating at interdendritic zones in the substrate. In the overlay coated SRR99 cracks continue to initiate almost up to the end of the cyclic life, achieving maximum crack number densities which exceed the crack number density in uncoated SRR99 by an order of magnitude at low strain ranges. Irrespective of the applied strain range initiation occurs in the coating, either at pre-existing porosity or induced by the roughness at the coating surface. During in-phase testing cracks invariably initiate at and grow from casting pores in the bulk of the specimen, irrespective of whether the specimen is bare or coated. In PtAl coated CMSX6 brittle cracking of the coating and inward growth of the coating cracks is a competing mechanism' in terms of life control.

In summary, coating of SRR99 and CMSX6 in general shortens the TMF life. Exceptions are the small life improvements relative to the uncoated materials for - 135°lag TMF cycling in the cases of the PtAl coated CMSX6 at low strain ranges and of overlay coated SRR99 at the high strain ranges. The beneficial effect of the diffusion coatings on crack initiation measured at the low applied strain ranges for'- 135°lag TMF cycling would suggest a positive/neutral effect of the coating on TMF life at strain ranges <0.6%.

3.1.3. Crack growth in TMF

The major part of the TMF life is spent in crack growth. In the -135°lag cycle tests, naturally initiated cracks grow in stage II in the coating and in the substrate material prior to turning to stage I late in life. At strain ranges in excess of about 1 % large scale slip on a preferred slip plane may trigger cracks to initiate and grow in stage I, in particular in uncoated material. During in-phase tests cracks invariably grow in stage II from casting pores in the bulk of the specimen, in an environment shielded from oxidation until the crack fronts break the surface. For - 135°lag cycling, the observations suggest a crack growth mechanism of the substrate material whereby oxide films, repeatedly formed in the high temperature part of the cycle, are broken by crack extension under the high tensile stresses prevailing at the intermediate/low temperature end of the cycle, giving rise to a flat stage 11 fracture path. At larger depths, the cracks grow by local crystallographic failure along alternating {111 } facets and the oxidation rate fails to match the crack depth increment per cycle.,

Widely different growth rates are measured for individual cracks in a given crack population. Apart from indivual growth, cracks also extend by means of coalescence with other cracks. An example of the length increments of all the cracks measured on a single test specimen are shown in fig.4, each symbol type representing the growth history of a different crack. The frequency of crack coalescence depends on' the crack number density, as shown for example in fig.5 for the growth history of the major crack for the - 135°lag,$R=-\infty$,$\Delta\varepsilon_m=0.7\%$ test condition. In the uncoated SRR99, the major crack grows individually at an average rate of the order of 6.10-8 m/cycle prior to accelerating at $N/N_f\approx 2/3$. Beyond $N/N_f\approx 2/3$, coalescence with two other cracks largely contribute to rapidly increasing the crack extension rate towards the end of the specinien life. In the NiAl coated specimen the steep increase of the crack extension rate at $N/N_f\approx 0.3$ is associated with the advent of crack coalescence, five such events being indicated on the crack growth curve whilst three more occur late in life. The crack growth history of the $\Delta\varepsilon_m=0.7\%$ test on the CoNiCrAlY coated specimen involves the running together of a total number of 22 cracks, some of the corresponding coalescence events being marked in fig.5. The result is a rapidly increasing overall crack growth length.

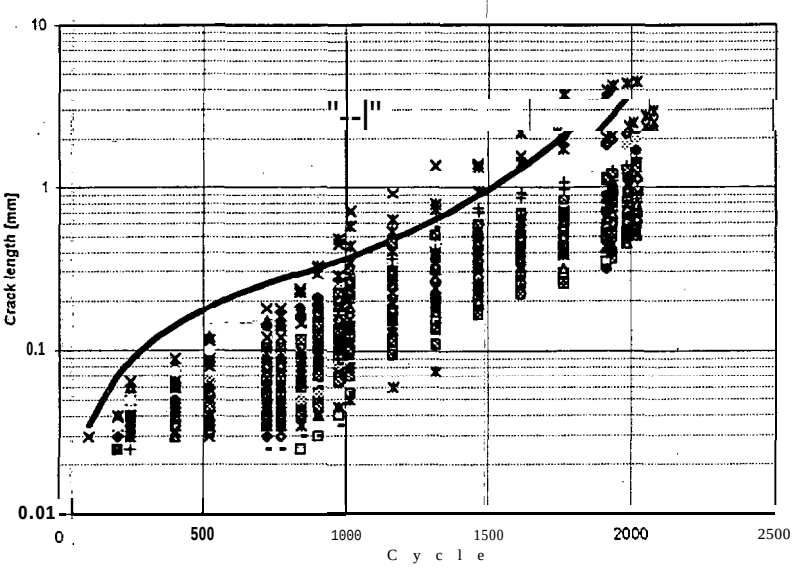

Fig.4 Growth history of different cracks in an uncoated SRR99 specimen TMF tested - 135 °lag, R=-∞, $\Delta\varepsilon_m$=0.7%. Each symbol type represents a different crack. The solid line is the crack growth history predicted by the model (see section 3.2.2)

The frequently observed life reduction due to the coating during -135°lag loading is associated with crack growth phenomena rather than with crack initiation effects. One major mechanism by which" coatings increase the overall rate of crack extension is through an enhanced frequency of crack coalescence events, triggered by the much higher crack number densities achieved in the coatings relative to uncoated materials. Another major mechanism operates at strain ranges in excess of 0.8% during -135°lag cycling, and is related to the already mentioned brittle failure of diffusion coatings which gives rise to long shallow edge cracks spanning the entire width of the specimen. The life reduction associated with the brittle mode of coating cracking can be explained in fracture mechanics terms.

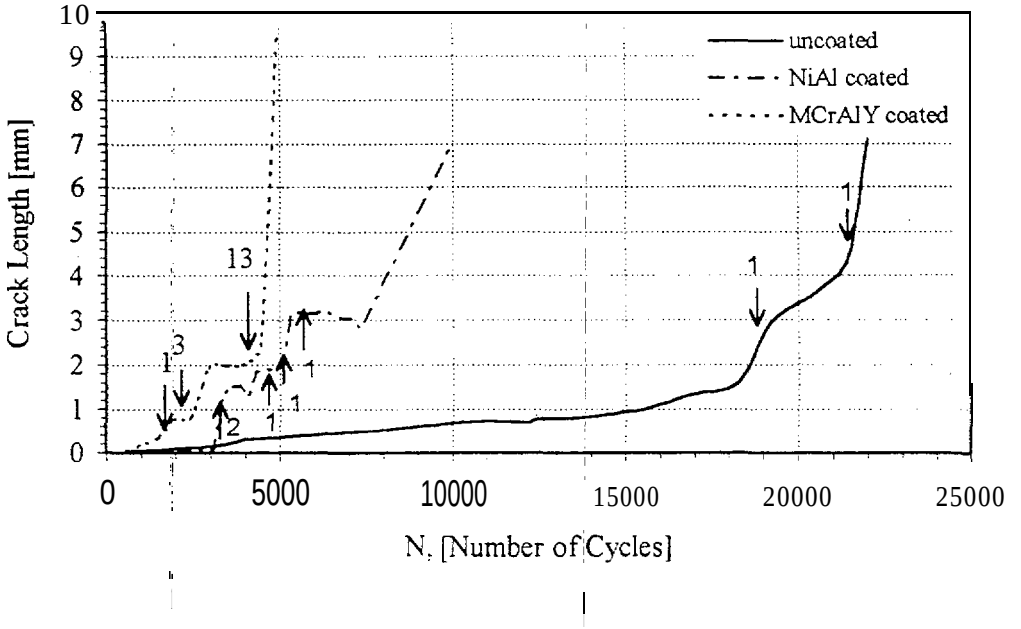

Fig. 5. Growth history of the major crack with cycle number N for - 135 °lag, R=-oo, $\Delta\varepsilon_m$=0.7% testing (SRR99).

The geometry factor F in the expression of the stress intensity factor is F=1.12 for an edge crack and F=0.66 for the deepest point on the front of the penny shaped cracks in uncoated material. Assuming a Paris equation for crack growth, the lives spent in propagating such cracks between the same initial and final depths are related through the expression

$$N_{f,line}/N_{f,Point} = (F_{Point}/F_{line})^n \quad (2)$$

Typical values of the Paris' "exponent n of 2 and 3 produce a ratio of cycles to failure of 0.34 and 0.2, respectively, indicating that the growth of brittle line cracks could lead to lives between 3 to 5 times shorter than the life of an uncoated specimen. In addition, the number of cycles for brittle crack initiation is smaller than that for initiating a penny shaped crack, the "' initial crack depth a_0 of line initiated cracks is of the order of the coating. thickness while a_0 of penny shaped cracks is much smaller, and the depth over which the line crack has to extend compared to the point initiation crack in order to cover equal fracture surface areas at specimen failure is approximately half. Each of these factors contributes to the observed life reduction in NiAl coated specimens at high strain ranges. A comparable life reduction mechanism operates during the in-phase loading with holdtimes of PtAl coated CMSX6. Long brittle cracks initiate in the coating and grow inwards, competing with the cracks growing from the casting porosity in the bulk of the substrate material and thereby substantially reducing the life of the coated specimens. The small yet consistent life reductions noted in coated versus uncoated materials in, many of the other in-phase loading conditions can not be explained within the context of the above mentioned mechanisms.

The coating induced reduction of the TMF life of coated versus uncoated SRR99 and CMSX6 is thus intimately related to cracking of the coating. Crack formation in the coating is governed by the fracture resistance of the coating material, which is controlled by its chemical composition and microstructure, and by the loading conditions, which are controlled by the TMF cycle and by the residual stress in the coating. The stress concentration at the porosity existing in the overlay coatings is responsible for initiating the cracks in the - 135°lag loading case. In the diffusion coatings, the microstructure in the as received condition depends on the coating thickness and,, on the chemical composition pf the substrate. The occurrence of a martensitic transformation with its associated negative volume change related to the cooling down of the ordered β-NiAl phase during TMF testing [18] is held responsible for initiating cracks in the NiAl coatings under specific TMF cyclic conditions.

In summary, the major part of the TMF life is spent in growing multiple initiated cracks by a mechanism of oxidation assisted fatigue early in life. The presence of a coating generally speeds up the rate of crack extension, which involves different mechanisms for different TMF loading conditions and coatings. Crack growth can accelerate as the result of crack coalescence, the frequency of coalescence and hence the crack extension rate depending on the density of initiated cracks and thus on the type of coating. The brittle failure of diffusion coatings during - 135°lag cycling at applied strain ranges in excess of approximately 0.8% provides another crack growth rate enhancing mechanism.

3.1.4. Isothermal crack growth

Almost equal crack propagation rates are observed for SRR99 and CMSX6 at temperatures below approximately 800°C and AK values in excess of 12 MPa$\sqrt{m}$. In this temperature regime the crack growth rate is fatigue controlled. Thermally activated processes do not contribute to crack propagation. At lower stress intensity factor ranges the crack growth rate of SRR99 deviates considerably from the Paris line, indicating the approach of a threshold. At 900°C the behaviour changes drastically. At the upper end of the AK range the crack growth rates of both materials approach one another, yielding appreciably higher growth rates as compared to the tests at intermediate temperatures as the result of oxidation effects. At 900°C the crack propagation rate of SRR99 is an order of magnitude smaller than that of CMSX6 at AK=1O MPa$\sqrt{m}$ as the result of SRR99'S higher threshold value for crack growth, which is thought to be due to oxide induced crack closure. Crack growth rates of SRR99 at 105O"C are shown for different R-ratios and loading frequencies in fig.6.

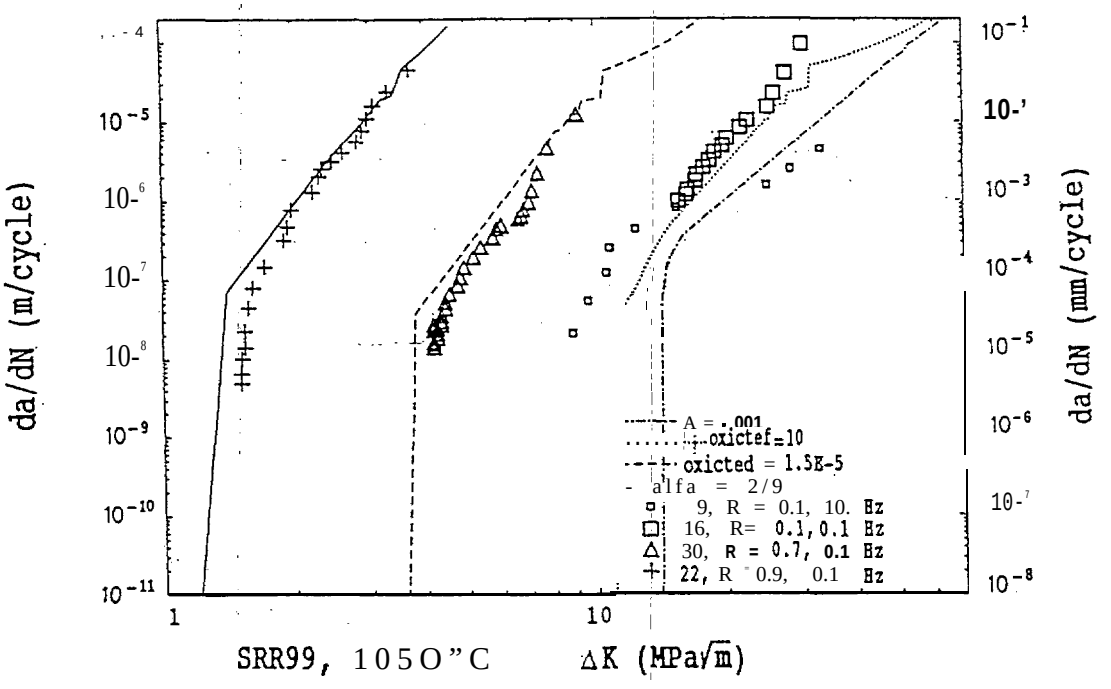

Fig.6 Experimental data and comparison between data and model predictions for the isothermal crack growth of SRR99 at 105O"C.

3.2. MODELLING

In view of the fact that the major fraction of the, life under TMF cycling conditions is concerned with crack' growth, crack propagation modelling is the appropriate route towards life prediction. The construction of an isothermal crack propagation model was considered relevant as a precursor to the modelling of the life under TMF conditions.

3.2.1. Isothermal crack propagation model

"A model that rationalises the experimental results and accounts for the experimentally observed strong interaction between fatigue and oxidation was developed. The fatigue term is modelled in terms of crack tip plastic blunting. The influence of 'oxidation is twofold: (i) brittle failure of the oxide scales contributes to crack *growth* during the crack opening phase, and (ii) the oxide scales also wedge the crack thereby modifying the fatigue term through a crack closure effect. This effect provides the interaction term between both 'mechanisms of crack propagation.

The fatigue crack growth term is assumed to correspond to a mechanism of crack tip plastic blunting,

$$(da / dN)_{fatigue} = C_o \delta^{n_o} \quad (3)$$

where d is the crack tip opening displacement, and C_o and n_o are material constants assumed to be temperature independent. For a power law hardening material, the expression for d was obtained by McMeeking [25] as

$$\delta = 0.6\,(K^2/E\sigma_0)[2(1+\nu)(1+n)\sigma_0/(\sqrt{3}En)]^n = n^*(K^2/E\sigma_0) \quad (4)$$

where K is the stress intensity factor, E is the Young's modulus, ν is the Poisson's ratio, σ_0 is the yield stress and n is the hardening exponent. Therefore, n* is a temperature dependent material constant. From Eqs. (3) and (4), the fatigue crack growth rate is obtained

$$(da/dN)_{fatigue} = CO\,(n^*/E\sigma_{cyclic})(AK)^{zn}o = C(\Delta K)^{2n_o} \quad (5)$$

where AK is the stress "intensity factor range in fatigue, σ_0 has been replaced by the cyclic yield stress, σ_{cyclic}, and the constant C is now temperature dependent.

The contribution of oxidation to crack growth is modelled through a twofold effect, see Fig. 7. Brittle oxide scales may fail at the tip of the growing crack (an enhanced oxidation zone), accelerating the crack growth through the term $(da/dN)_{oxidation}$. On the other hand, these oxide scales may wedge the crack and reduce the fatigue effective stress intensity factor range through a crack closure effect, K_{Cl}. In order to take account of crack closure, the stress intensity factor range in Eq. (5) is replaced by an effective stress intensity factor range for fatigue crack propagation: . . .. ----

$$(da/dN)_{fatigue} = C(\Delta K_{eff})^{2n_o}$$

$$\Delta K_{eff} = K_{max} - max(K_{min}, K_{Cl}) \quad (6)$$

An approximate-elastic solution due to Suresh et al. [26] for K_{Cl} when the crack is wedged by a rigid oxide scale is

$$K_{Cl} = dE/[4\sqrt{\pi l}(1-\nu^2)] \quad (7)$$

where d is twice the compacted oxide scale thickness over the original crack surface and $2l$ is the crack growth per cycle, $2l = (da/dN)_{total}$. Then

$$K_{Cl} = AeE/[(1-\nu^2)\sqrt{(da/dN)_{total}}] \quad (8)$$

where e is the oxide scale thickness before being compacted and A is introduced as a temperature dependent constant.

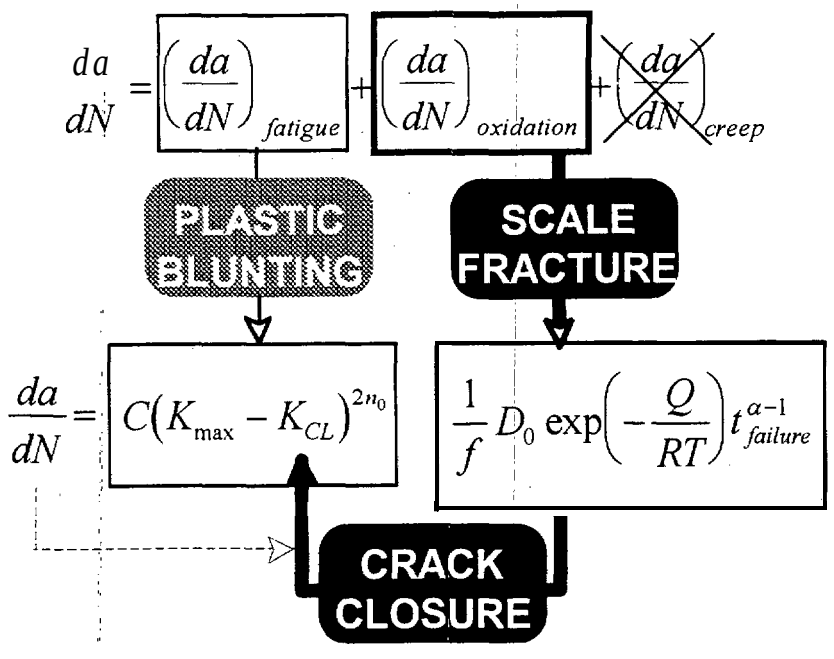

Fig.7 Schematic of the proposed fatigue-oxidation crack growth model

In the static case, the oxide scale thickness,e,is given by an Arrhenius type law

$$e = Dt^{a} = D_0 \exp(-Q/RT)\, t^{\alpha} \quad (9)$$

where t is the time, T is the absolute temperature, R is the gas constant (R = 8.314 J/molxK), Q is an activation energy and D_0 is a constant. Typical values for the time exponent a in this type of materials are 1/2, 1/4 [27] and 1 in the initial stages of oxidation [28]. It is assumed that in the oxide scale a major defect of size a is present, where a is proportional to the scale thickness e i.e. a = Be. The stress intensity factor at the tip of such a microcrack, K_{local}, is

$$K_{local} = \beta\sigma_{local}\sqrt{\pi a} = \beta.(K(t)/\sqrt{2\pi r}).\sqrt{\pi Be} = \beta.\sqrt{BD/2r}.K(t)t^{\alpha/2} = F\sqrt{D}K(t)t^{\alpha/2} \quad \text{(lo)}$$

$$F = \beta\sqrt{B/2r}$$

where β is a crack shape factor, r is a critical distance from the crack tip, and K(t) is the remote stress intensity factor for the main crack. When this local stress intensity factor reaches the oxide scale toughness, $K_{IC}^{(ox)}$, the microcrack propagates into the maior crack and fractures all the oxide scale thickness, then blunting at the ductile substrate. $K_{IC}^{(ox)}$ values of 0.41 and =1.61 MPa$\sqrt{m}$ have been reported for Ni0 at room temperature and at 900°C, respectively [29]. The critical time for failure of the oxide scale, t_f, is then given by the condition

$$K_{local} = K_{IC(ox)} \rightarrow K_{IC}^{(ox)} = F\sqrt{D}K(t_f).\ t_f^{\alpha/2} \quad (11)$$

Therefore, the mean crack growth rate is

$$(da/dt)_{ox} = [e(t=t_f)]/t_f = D\, t_f^{\alpha-1} \quad (12)$$

Finally, using Eqs.(12) and (9), the proposed equation for the oxidation crack growth term is

$$(da/dN)_{ox} = (1/f).(da/dt)_{ox} = (1/f).D_0.\exp(-Q/RT)t_f^{\alpha-1} \quad (13)$$

where f is the cycle frequency, Do and Q are material constants, and t_f is determined from the condition (11).It is reasonable to assume that rupture of the oxide scale only occurs if the crack opens. Therefore, this contribution to crack propagation, Eq.(13), will be added to the other fatigue terms provided that $\Delta K_{eff}>0$.

The analysis of the experimental results reported by Yang [30] for creep tests carried out at 105O"C (the highest temperature in the present Analysis) on SRR99 single crystal in the <001> direction indicates that the creep contribution to the total crack growth rate is one order of magnitude smaller than that due to the other crack propagation components. The creep behaviour of CMSX-6 is assumed to be similar to that of SRR99, and therefore its contribution to the total crack propagation rate will be also negligible compared to the other crack growth terms.

In order to fit Eq.(5) for the fatigue term, data from the tests at the lowest temperature (500°C) were used to obtain the constants C_0 and n_0 for both materials. Two different crack propagation modes were observed: through the y channels and along the crystallographic <111> planes. The crack will choose the path that relaxes more energy. that is the one with the highest growth rate. Regarding the oxidation crack growth term, data at the highest temperatures were used to fit the constants α, Do and Q in Eq.(13). The resulting constants are summarised in Table 1, when da/dN is expressed in m/cycle, K is in MPa$\sqrt{m}$ and the time is in seconds. Note that, for the propagation through the y channels, the Paris' exponent, 2 n_0, for both materials is close to *2*, typical of a crack tip plastic blunting mechanism. The propagation along the e111> planes occurs by cutting the brittle γ' precipitates, so this crack propagation mode has a brittle contribution. resulting in higher values for the Paris' exponent. As an example of the results, Fig. 6 shows the comparison between the model predictions and the experimental data for SRR99 at 105O"C.

TABLE 2. Parameters of the isothermal crack growth model

		CMSX6	SRR99
Fatigue (γ) channels	c_o	4.251×10^{-2}	4.267×10^{-2}
	n_o	1.074	1.074
Fatigue (crystallographic)	c_o	1.096×10^{-5}	4.000×10^{-5}
	n_o	2.320	2.320
Oxidation	α	0.40	0.22
	D_o	1.616×10^{-2}	1.025
	Q(kJ/mol)	94.5	122.7

Summarizing, the effect of oxidation on crack growth is twofold: brittle oxide scales may fail at the crack tip and the oxide scales may also wedge the crack, then producing a strong interaction between fatigue and oxidation crack growth through a crack closure effect. Whereas the contribution of crack tip plastic blunting to crack growth rate is very similar in both materials, the oxidation behaviour of SRR99 and CMSX-6 differs significantly. SRR99 is more prone to oxidation and crack closure than CMSX-6. Thus, depending on the temperature, frequency and loading ratio, one material will exhibit a better fatigue response than the other. The proposed model fits and explains, reasonably well the different fatigue crack propagation behaviour found for CMSX-6 and SRR99 in a wide range of temperatures (500 to 105O"C) frequencies (0.001 to 20 Hz, with and without hold times) and loading ratios R (O to 0.9).

3.2.2. Life prediction model for thermo-mechanical fatigue

The analysis of TMF test images showed that the failure of uncoated specimens in -135°lag cycling is due to the multiple initiation of cracks at oxidation spikes on the sample surface, followed by growth and crack coalescence. The plots of crack length versus number of cycles reveal a transition in' the crack evolution which suggests a change in the crack growth mechanism. Therefore, TMF life of a single crystal superalloy was modelled as a function of two damage mechansms: oxidation and fatigue. The model assumes that TMF crack growth can be represented by two stages, each stage being governed by a different damage mechanism: oxidation through the first stage and fatigue during the second. The model aims to reproduce the observed behaviour of the TMF cracks through the growth of" a unique equivalent or characteristic crack which represents the general evolution of the TMF cracks leading to failure for the different testing conditions.

Oxidation is assumed to dominate crack growth behaviour during the early testing period. An initiation site enhances local oxidation, followed by the growth of an oxide layer until it reaches a critical thickness and fractures. This allows the oxygen to penetrate and form a new oxide layer at a deeper level. Again, once a critical thickness is reached, fracture of the oxide layer occurs and the diffusion process restarts.The growing mechanism is mathematically represented as follows:,

$$a = A\,\sigma^{\beta}_{max} N^{\alpha} \qquad \text{"(14)}$$

were a is the crack length, σ_{max} is the maximum tensile stress, and N is the number of cycles. The oxidation kinetics is linear (α=1) when the material does not present any impedance to the oxidation, which has been reported to be true during the first oxidation stage in nickel base superalloy [28]. The dependence of the peak stress represents the effect of the applied load on the successive cracking of the oxide layer.

The fatigue mechanism is modelled by means' of a Paris' law defined in terms of the effective stress intensity factor which accounts for the influence of crack closure due to oxidation (K_{Cl})

$$da/dN = C(K_{max} - K_{Cl})^n \quad (15)$$

The crack closure effect is described through an equation of the form

$$K_{Cl} = B/|\sigma_{min}|^{\beta} \quad (16)$$

This dependence. on the minimum stress, σ_{min}, is consistent with the idea that the larger the compressive stress is: the smaller the crack closure effect. This phenomenon has been experimentally observed and is related to the fact that compressive stresses tend to smooth down surface defects and, consequently, reduce crack closure.

The transition between oxidation and fatigue dominated crack propagation is assumed to occur when the crack reaches a- specific microstructural size [18,19]. A regression analysis between the number of cycles to transition and the peak stress of each test provides the numerical from of Eq. (14).

$$a = (a_{trans}/3.5x10^{10})\,\sigma^{2.58}_{max}\,N \quad (17)$$

where σ_{max} is expressed in MPa, and a_{trans} and a are in the same units. The transition size was calculated as the arithmetic mean of the experimentally measured sizes, resulting in a value of a_{trans}=0.288 mm.The constants C, n, B and b were calculated by means of a regression analysis of the cycles to failure versus the result of integrating the effective stress intensity factor over the testing time. The resulting equations are

$$da/dN = 2x10^{-9}(K_{max} - K_{Cl})^2 \quad (18)$$

were K is in MPa√m and da/dN is in m/cycle, and

$$K_{Cl} = 337/|\sigma_{min}|^{0.7}(uncoated) \qquad K_{cz} = 139/|\sigma_{min}|^{0.64}(coated) \quad (19)$$

for uncoated and coated specimens,were K_{Cl} is expressed in MPa√m and the stresses in MPa.

Using the above equations, it is possible to reproduce the TMF crack evolution for different testing conditions. As a example, Fig. 4 shows the comparison between the predicted crack evolution and the experimental data in a particular test. Figure 8 shows the predicted lives versus the actual lives for all the - 135°1ag tests, coated and uncoated. Results satisfy the initial

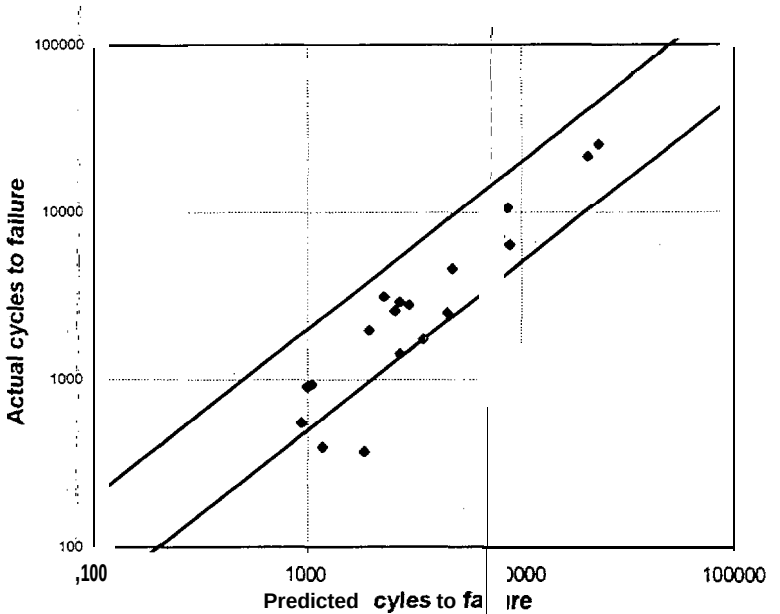

Fig.8 Comparison of' predicted and actual lives for he -135°lag TMF tests in coated and uncoated SRR99

expectation of reproducing the general trend of the crack leading to failure. A good correlation between predicted and actual lives is observed except for two tests which showed complete crystallographic failure and lay outside the error bands. The model accounts for the differences in life between uncoated and coated specimens (in -135°lag TMF testing of bare and aluminide coated SRR99) through the lower crack closure effect in coated samples where the oxidation effect is not as important as in the uncoated samples, and consequently the crack grows faster. The model, as a first approximation, is able to reproduce the main crack growth behaviour by emphasizing the role of oxidation in the crack growth mechanism.

4. CONCLUSIONS

The main conclusions of the research project are:

1. The TMF test mimics the in-service conditions of critical blade volume elements, thereby enabling the assessment of the associated damage and failure mechanisms and of the stress-strain-temperature relationship prevailing within the blade volume element.

2. The inelastic strain accumulation within each cycle and on a cycle-by-cycle basis gives rise to different damage mechanisms for different TMF cycle types. This precludes the formulation of a generally applicable life prediction model for TMF.

3. Cracks initiate very early in the cyclic life. The number of cycles for crack initiation at each applied strain range, the crack number density and the initiation mechanism depend on the TMF cycle type and on the presence and type of coating. Diffusion coatings in particular have a large beneficial effect on crack initiation at low applied strain ranges for cycling under - 135°lag conditions.

4. The major part of the TMF life is spent in growing multiple initiated cracks by a mechanism of oxidation assisted fatigue early in life. The presence of a coating generally speeds up the rate of crack extension, which involves different mechanisms for different TMF loading conditions and coatings. Crack growth can accelerate as the result of crack coalescence, the frequency of coalescence and hence the crack extension rate depending on the density of initiated cracks and thus on the type of coating. The brittle failure of diffusion coatings during - 135°lag cycling at applied strain ranges in excess of approximately O. 8% provides another crack growth rate enhancing mechanism.

5. In terms of TMF life, the presence of the coating has a detrimental effect in the majority of the investigated single crystal/coating combinations and test conditions. A life lengthening effect of the coating is observed in the case of@ MCRA1Y coating on SRR99 at strain ranges exceeding 0.9%, and for the PtA 1 coating on CMSX6 at strain ranges below 0.770. The largest life reduction as the result of coating occurs in overlay coated SRR99 at low applied strain ranges. The extent of the coating-induced changes in TMF life depends on the TMF cycle type, on the type of coating, on the substrate material and on the applied strain range. Overall, the diffusion coatings outperform the overlay coatings in terms of their effect on the TMF life.

6. In the early stages of life under -135° lag cycling, inelastic deformation concentrates in the interdendritic zones of the single crystal, resulting in crack initiation at stress raisers such as carbides/porosity in uncoated specimens. Damage in diffusion coatings is exacerbated by the presence of the strain concentrating at interdendritic zones (based on observations on NiA1 coated SRR99). In-phase loading promotes crack initiation at casting porosity in the bulk of the single crystal substrate. Based on these observations the following life improving measures can be suggested:
   - hipping of the single crystal substrate in order to reduce the volume fraction of casting porosity. Hipping of overlay coated blades may have an even larger beneficial effect in that the volume fraction of the porosity in the. overlay coating is simultaneously reduced. An additional benefit in terms of delaying crack initiation in overlay coatings may be gained by a finer finish of the coating surface.

- homogeneisation of the structure of the single crystal at the scale of the dendrites/interdendritic zones.
- removal of carbon, thereby inhibiting the formation of carbides which are believed to act as crack initiating features.
- preferential matching of the secondary crystallographic orientation with the blade geometry in diffusion coated blades.

7. A series of issues not addressed in this Brite project requires investigation in order to enable optimizing of the performance of coated single crystal blades and to extend mechanism-informed life modelling. These relate to the precise mechanisms at the scale of the microstructure of the coating and of the single crystal substrate of crack initiation and growth, to understanding the-effect of the coating on life under in-phase cycling, to rationalizing the difference in behaviour between different coatings, as well as to the influence of a range of variables on crack initiation, crack growth and life under TMF loading (including the maximum and minimum cycle temperatures, the loading/unloading rate, pre-oxidation effects, and effects of coating thickness/secondary crystallographic orientation of the substrate)

8. A mechanism-informed fatigue-oxidation model is proposed for the case of isothermal LCF crack propagation. The model proved to be" very robust and has the following attributes:
   - oxidation plays a major role in fatigue crack propagation in single crystal nickel base superallo ys SRR99 and CMSX-6. The effect of oxidation on crack growth is twofold: brittle oxide scales may fail at the crack tip and the oxide scales may also wedge the crack, then producing a strong interaction between fatigue and oxidation crack growth through a crack closure effect. Isothermal crack growth of CMSX-6 and SRR99 can be rationalised in terms of two interacting crack propagation terms, one attributed to crack tip plastic blunting and the other to the brittle failure of the oxide scales. Creep seems to play a minor role.
   - the contribution of crack tip plastic blunting to crack growth rate is very similar in both materials.
   - the oxidation behaviour of CMSX-6 and SRR99 differs significantly, the latter being more prone to oxidation and crack closure than CM SX-6. Thus, depending on the temperature, frequency and loading ratio, one material will exhibit a better fatigue response than the other.
   - the proposed model fits and explains the different fatigue crack propagation behaviour found for CMSX-6 and SRR99 in a wide range of temperatures, 'frequencies and loading ratios R.

9. A similar mechanism-informed approach was taken to modelling the -135°lag TMF lives. The model accounts for the differences in life between uncoated and coated specimens through a smaller crack closure effect in coated material. The oxidation effect in coated samples is less important, and hence the crack grows faster in coated material. The model reproduces reasonably well the main crack growth behaviour by emphasizing the role of oxidation in the crack growth mechanism. Although several other factors should be taken into account for a more realistic representation of the experimentally observed processes, such as the influence of the microstructure and the interaction between cracks, the approach taken enables the prediction of TMF lives within a factor of two for -135°lag TMF testing of bare and aluminide coated SRR99.

5. ACKNOWLEDGMENTS

This work has been performed as part of the Brite-Euram project BE3338-89 with financial support from the EC, coordinated by Rolls-Royce (UK). All the participants gratefully acknowledge the part played in this programme by the European Commission, and would particularly like to thank Dr. N.E.W.Hartley and Dr. H. H.Walther for their help and forbearance in all matters relating to the project.

REFERENCES

1. J.C.Newman,Jr, I. S.Raju, Stress-intensity factor equations for cracks in three-dimensional finite bodies, *Fracture Mechanics : Forteenth Symposium, ASTM STP 791,* J. C. Lewis and G. Sines (eds.), ASTM, Philadelphia (1983), pp.I-238-I-265,2.

2. T.N.Rhys-Jones, J.Bressers, M.Buckley, Thermo-mechanical fatigue of advanced gas turbine *materials,Symposium on therm-mechanical fatigue,* Institute of Metals, Feb. 12,1992.

3. J. Bressers,T.Rhys-Jones, J.Estevas-Guilmain, A.Franks, TMF testing of high-temperature materials, *Symposium on thermo-mechanical fatigue, Institute* of Mets.ls,Feb. 12,1992.

4. J.Bressers, J.Timm, S.Williams, A.Bennett, E.Affeldt, Effects of cycle type and coating on the TMF lives of a single crystal nickel based, gas turbine alloy, in *Thermo-Mechanical Fatigue Behaviour of Materials:* 2nd Volume, ASTM STP 1263, Michael J. Verrilli and Michael G.Castelli (Eds.), American Society for Testing and Materials, Philadelphia% 1995.

5. J.Bressers, J.M.Martinez-Esnaola, A. Martin-Meisozo, J. Timm, M. Arana-Antelo, Coating effects on crack growth in a single crystal nickel-based alloy during thermo-mechanical fatigue, in *Thermo-Mechanical Fatigue Behavior of Materials:* 2nd Volume, ASTM STP 1263, Michael J. Verrilli and Michael G. Castelli,(Eds.), American Society for Testing and Materials, Philadelphia, 1995.

6. D.J.Arrell, J. L. Vallés, Interracial dislocation based criterion for the prediction of rafting behaviour in superalloys, *Scripts metall.et mater.*30,1994, *149.*

-1. J. L. Vanes, D. J. Arrell, Monte Carlo simulation of anisotropic coarsening in nickel base superalloy, *Acta metall et mater.* 42,1994, 2999.

8. J. L. Vanes, D.J.Arrell,J.Bressers, Misfit dislocations and anisotropic coarsening in superalloys", *Archives of Mechanics, 47(3), 1995,601-15.*

9. D.J.Arrell, J. L. Vallés, A model for microstructural evolution in superalloy subjected to an applied stress, *Localized Damage III: Computer aided assessment and control.* eds. M. H. Aliabadi et al., Computational Mechanics Publications, Southampton,1994.

10. J. L. Valles, D.J.Arrell, Mechanism based modelling of anisotropic coalescence in superalloy, *Proceedings of CODATA '94: Materials and Structural Properties,* 18-22 sep.1994, Chambéry, France:

11. P. Moretto, J. Dressers, Them-m-mechanical fatigue degradation of a nickel aluminide coating on a single crystal nickel based alloy, accepted for publication to *Journal of Materials Science*

12. D.J.Arrell, K.M.Ostolaza, J. L. Vallés, J. Dressers, Solidification structures and post-fatigue precipitate morphology in a single crystal superalloy, in Proc.International Symposium *Fatigue under Thermal and Mechanical Loading,* J.Bressers, L. Rémy, M. Steen and J. L. Vallés, (eds.), Kluwer, (1996), pp.295-304.

13. K.M.Ostolaza, D.J.Arrell, J. L. Vallés, J. Dressers, Effect of substrate crystal orientation on the microstructure and fracture properties of nickel-alumunide coatings on superalloys subjected to TMF, in Proc.International Symposium *Fatigue under Thermal and Mechanical Loading,* J.Bressers, L. Rémy, M. Steen and J. L. Vallés, (eds.), Kluwer, (1996), pp.305-3 14.

14. P.Johnson, J. Dressers, Characteristics of a population of naturally initiated cracks that evolve during TMF testing of bare and aluminide coated SRR99, in Proc.International Symposium *Fatigue under Thermal and Mechanical Lading,* J. Dressers, L.Rémy, M. Steen and J. L. Vallés, (ids.), Kluwer, (1996),pp.315-326.

15. K.M.Ostolaza, J.L.Vallés, J. Dressers, Evolution of a nickel-aluminide diffusion coating on a single crystal superalloy during TMF, in 2nd International Conference *Surface Treatment '95*, Milano, June 7-9,1995.

16 J. Dressers, D.J.Arrell, K.M.Ostolaza, J. L. Vallés, Effect of coatings on precipitate rafting in supers.lIoys, in 7th International Conference on *Mechanical Behaviour of Materials ICM7*, May 28-June 2, 1995, The Hague, The Netherlands

17. E. Affeldt, J.Timm, A.Bennett, Importance of crack growth to damage under TMF loading in Proc.International Symposium *Fatigue under Thermal and Mechanical Loading,* J.Bressers, L.Rémy, M. Steen and J. L. Vallés, (eds.), Kluwer, (1996), pp. 159-168.

18. M.Arana, Fatiga termomecanica de una superaleacion monocristalina de base niquel (SRR99). Comportamiento mecanico y prediction de viola", Ph.D. Thesis, Esuela Superior de Ingenieros Industrials de San Sebastian, Universidad de Navarra,(1995).

19. M.Arana, J.M.Martinez-Esnaola, J.Bressers, Crack propagation and life prediction in nickel-based superalloys under TMF conditions, in Proc.International Symposium *Fatigue under Thermal and Mechanical Lading,* J. Dressers, L.Rémy, M. Steen and J. L. Vallés, (eds.), Kluwer, (1996),pp.393-402.

20. A.Martin-Meizoso, J.M.Martinez-Esnaola, M. Fuentes, Apantallamiento de grietas en fatiga, *Anales de Mecánica da la Fractura, 11,(1994),81-88.*

21. M.Arana, J.M.Martinez-Esnaola, M. Fuentes, Agrietaminto del recubrimiento de un monocristal de base niquel en fatiga termomecánica, *Anales de Mecánica da la Fractura,* 11,(1994),164-169.

22. M. Arana, J. M.Martinez-Esnaola, M. Fuentes, Predicción de viola en un monocristal de base niquel en fatiga termomecánica, *Anales de Mecánica de la Fractura, 12,(1995),373-378.*

23, J. M.Martinez-Esnaola, M. Arana, J.Bressers, J.Timm, A. Martin-Meizoso, A.Bennet, E.Affeldt, Crack initiation in an aluminide coated single crystal during thermo-mechanical fatigue, in *Thermo-Mechanical Fatigue Behavior of Materials:* 2nd Volume, ASTM STP 1263, Michael J. Verrilli and Michael G. Castelli,(Eds.), American Society for Testing and Materials, Philadelphia, 1995.

24. A. Martin-Meizoso, J.M.Martinez-Esnaola, M. Fuentes-Pérez, Interactive effect of multiple crack growth on fatigue, Theoretical and Applied Fracture Mechanics, 23,(1995),219-233.

25. R. M. McMeeking, Finite deformation analysis of crack-tip opening in elastic-plastic materials and implications for fracture, J. Mech.Phys.Solids, 25,(1977),357-38 1.

26. S. Suresh, D.M.Parks, R.O.Ritchie, Crack tip oxide formation and its influence on fatigue thresholds. *Fatigue Thresholds, Fundamentals and Engineering Applications,* Vol.1. J. Backlund. A.F.Blom and C.J.Beevers. (Eds.) Engineering Materials Advisory Servies Ltd. (EMAS) UK.,(1982) pp. 391-408.

27. M. Reger, L.Remy, Fatigue oxidation interaction in IN 100 superalloy. Metall. Trans. A.19a, (1988), 2259-2268;

28. T.E.Strangman, Thermal-mechanical fatigue life model for coated superalloy turbine components, Superalloy 1992, S. D. Antolovich,R.W Stusrud, R. A. Mackay, D. L. Anton,T.Khan, R.D.Kissinger, D.L.Klarstrom, (Eds.), The Minerals, Metals & Materials Society,(1992). pp. 795-804.

29. M. M.Nagl, S. R. J. Saunders, W. T. Evans and D.J. Hall, The tensile failure of nickel oxide scales at ambient and at growth temperature, Corrosion Science, 35,(1993),965-977.

30. R.Yang, Creep-fatigue crack growth in a nickel base superalloy, Ph.D. Thesis, Department of Mechanical Engineering. Imperial College of Science, Technology and Medicine, London, (1991).